Eur. Phys. J. B **15**, 133–141 (2000)

THE EUROPEAN PHYSICAL JOURNAL B

EDP Sciences

Lattice Boltzmann simulation of a binary fluid with different phase viscosities and its application to fingering in two dimensions

K. Langaas[1,a] and J.M. Yeomans[2]

[1] RF - Rogaland Research, PO Box 2503, 4091 Stavanger, Norway
[2] Department of Physics, Theoretical Physics, 1 Keble Road, Oxford OX1 3NP, UK

Received 25 May 1999 and Received in final form 19 November 1999

Abstract. A thermodynamically consistent lattice Boltzmann scheme for simulating the flow of a binary fluid is extended to allow the fluid components to have different viscosities. The approach is tested for the shear and Poiseuille flow of layered immiscible fluids and for the dispersion relation and the damping of a capillary wave. We then consider the fingering that results when a fluid is displaced by a less viscous fluid in a two-dimensional channel. The finger widths obtained match the results of Reinelt and Saffman [1], but differ somewhat from those of Halpern and Gaver [2] for capillary numbers above 2. A limiting finger width close to 1/2 is obtained for high capillary numbers and high viscosity ratios.

PACS. 47.11.+j Computational methods in fluid dynamics – 83.10.Lk Multiphase flows – 66.20.+d Viscosity of liquids; diffusive momentum transport

1 Introduction

The lattice Boltzmann method is an approach for solving the Navier-Stokes' equations of fluid flow [3]. It can be viewed either as a slightly unusual finite-difference scheme or as a discretization of a simplified Boltzmann equation. The latter interpretation allows the simulation variables to be identified as one-particle distribution functions. These move around the lattice *via* consecutive streaming and collision steps. The collisions conserve mass and momentum so the system obeys the continuum equations of fluid dynamics at sufficiently long times.

The lattice Boltzmann scheme consists mainly of local operations, and is ideal for parallel processing. Since no-flow boundaries are easily implemented, the method is especially suited to simulate flow in complex geometries, as, for example, multiphase flow in a porous medium.

Gunstensen *et al.* [4] extended the lattice Boltzmann method so that two immiscible phases could be simulated. By phenomenological collision and recoloring rules, a sharp interface between the two phases was obtained. Flekkøy [5] introduced a lattice Boltzmann scheme capable of simulating both the Navier-Stokes and the convection-diffusion equation in the one-phase region. Orlandini *et al.* [6,7] presented a similar, thermodynamically-consistent, model for two-phase systems. Here the equilibrium state minimizes a chosen free energy and the corresponding pressure tensor and chemical potential coupling to the density difference appear in the Navier-Stokes and convection-diffusion equations respectively. This permits the simulation of immiscible flow problems. This method has been successfully applied to various physical problems, such as spinodal decomposition [8] and flow in porous media [9].

In this article we extend the binary fluid model proposed by Orlandini *et al.*, so the two components can have different viscosities. Both Grunau *et al.* [10] and Rakotomalala *et al.* [11,12] have used the lattice Boltzmann method to study two-viscosity problems. Grunau *et al.* used a second order polynomial in $\Delta n/n$ (see below) to connect the bulk phase viscosities in the Gunstensen *et al.* model. Rakotomalala *et al.* extended Flekkøy's model, with the same "ideal" viscosity relation that is used in this paper. The important difference to our approach is that here the interfaces between the two phases are stable and have a thermodynamically consistent profile.

The computational scheme is described in the next section of the paper. The model, currently implemented in two dimensions, is checked against the test cases of the shear and Poiseuille flow of layered immiscible fluids where analytic results are available for comparison. These results are described in Sections 3.1 and 3.2 respectively. For shear and Poiseuille flow geometries the interface between the fluids is stationary in time. To evaluate our method also for a moving interface problem with analytical predictions the dispersion and damping of a capillary wave is calculated in Section 3.3. Finally, in Section 3.4, the model is used to investigate the evolution

[a] e-mail: Kaare.Langaas@rf.no

of the finger that form when a fluid pushes a second fluid of higher viscosity in a two-dimensional channel.

2 The numerical approach

2.1 Thermodynamics

Before the implementation of two viscosities is explained, we summarize the fundamentals of the binary-fluid model used here. For more details, the reader is referred to references [6,7].

The binary fluid model is comprised of two ideal gases A and B with number densities n_A and n_B respectively and a repulsive $A-B$ interaction energy. The Helmholtz bulk free energy density at a temperature T is given by

$$\psi(n,\Delta n,T) = kT\left[\frac{n+\Delta n}{2}\ln\left(\frac{n+\Delta n}{2}\right) + \frac{n-\Delta n}{2}\ln\left(\frac{n-\Delta n}{2}\right) - n\right] + \frac{\varpi n}{4}\left[1-\left(\frac{\Delta n}{n}\right)^2\right] \quad (1)$$

where $n = n_A + n_B$ and $\Delta n = n_A - n_B$ are a convenient choice of independent variables. ϖ measures the strength of the interaction. For $kT < \frac{1}{2}\varpi$ the bulk system phase separates into two phases, with density differences $\pm\Delta n_0$. k is the Boltzmann constant.

To capture the surface tension, that is the excess free energy associated with an interface, we use the quasi- or local thermodynamic assumption that local values of the different thermodynamic potentials can be defined in an inhomogeneous system [13]. Assuming further that the total density is constant across the interface, the Helmholtz free energy for the inhomogeneous system can be written

$$\Psi = \int\left[\psi(n,\Delta n,T) + \frac{\kappa}{2}(\nabla\Delta n)^2\right]\mathrm{d}^3\mathbf{r} \quad (2)$$

where κ is a constant related to the surface tension. The chemical potential for the density difference and the stress tensor follow [14]

$$\mu_{\Delta n} = \mu^0_{\Delta n} - \kappa\nabla^2\Delta n \quad (3)$$

where

$$\mu^0_{\Delta n} = \frac{kT}{2}\ln\left(\frac{n+\Delta n}{n-\Delta n}\right) - \frac{\varpi}{2}\frac{\Delta n}{n} \quad (4)$$

and

$$\sigma_{ij} = p\delta_{ij} + \kappa\partial_i\Delta n\partial_j\Delta n \quad (5)$$

where

$$p = nkT - \kappa\left[\Delta n\nabla^2\Delta n + \frac{1}{2}(\nabla\Delta n)^2\right]. \quad (6)$$

The short notation $\partial_i \equiv \frac{\partial}{\partial x_i}$ and $\partial_t \equiv \frac{\partial}{\partial t}$ is used in this article. Note that the system satisfies the ideal gas law ($p_0 = nkT$) in the bulk phases away from the interface. The surface tension at a given point $\mathbf{r}_0$ is [14]

$$\sigma_{\mathbf{r}_0} = \kappa\int(\nabla\Delta n)^2\mathrm{d}\mathbf{r}_n \quad (7)$$

where the integral is performed through the interface along the interface normal.

2.2 The lattice Boltzmann scheme

The lattice Boltzmann approach is based on two sets of distribution functions $\{f_\alpha\}$ and $\{g_\alpha\}$, which evolve according to the lattice analog of the BGK-model of kinetic theory [15,16]. At each time step the distribution functions undergo a collision step followed by a streaming step

$$f_\alpha(\mathbf{r}+\mathbf{v}_\alpha\Delta t, t+\Delta t) - f_\alpha(\mathbf{r},t) = -\frac{\Delta t}{\tau_f}(f_\alpha - f^{(0)}_\alpha), \quad (8)$$

$$g_\alpha(\mathbf{r}+\mathbf{v}_\alpha\Delta t, t+\Delta t) - g_\alpha(\mathbf{r},t) = -\frac{\Delta t}{\tau_g}(g_\alpha - g^{(0)}_\alpha). \quad (9)$$

Here, $\mathbf{r}$ denote a discrete lattice node, Δt is the time-step, α denotes the different lattice directions, and $\mathbf{v}_\alpha$ denotes the lattice velocity vectors. The results presented in this paper are for a 9-velocity model on a square lattice with $\{\mathbf{v}_\alpha\} = v\{(0,0),(0,\pm1),(\pm1,0),(\pm\sqrt{2},\pm\sqrt{2})\}$ where $v \equiv \Delta x/\Delta t$ and Δx are the lattice velocity and spacing on the main (short) axes, respectively. τ_f and τ_g are relaxation times. The $\{f_\alpha\}$ determine the total number density and the macroscopic flow velocity $\mathbf{u}$, while the $\{g_\alpha\}$ give the number density difference

$$n \equiv \sum_\alpha f_\alpha, \qquad nu_i \equiv \sum_\alpha f_\alpha v_{\alpha i}, \qquad \Delta n \equiv \sum_\alpha g_\alpha. \quad (10)$$

The Latin index i represent the Cartesian i-component of a vector. Below the usual convention of summing over repeated Latin indices is assumed.

The thermodynamics is input through the equilibrium distribution functions $\{f^{(0)}_\alpha\}$ and $\{g^{(0)}_\alpha\}$. These are chosen to fulfill the following conditions

$$\sum_\alpha f^{(0)}_\alpha = n, \qquad \sum_\alpha f^{(0)}_\alpha v_{\alpha i} = nu_i, \quad (11)$$

$$\sum_\alpha f^{(0)}_\alpha v_{\alpha i}v_{\alpha j} = \sigma_{ij} + nu_iu_j, \quad (12)$$

$$\sum_\alpha g^{(0)}_\alpha = \Delta n, \qquad \sum_\alpha g^{(0)}_\alpha v_{\alpha i} = \Delta nu_i, \quad (13)$$

$$\sum_\alpha g^{(0)}_\alpha v_{\alpha i}v_{\alpha j} = \Gamma\mu_{\Delta n}\delta_{ij} + \Delta nu_iu_j \quad (14)$$

where Γ is a constant and σ_{ij} and $\mu_{\Delta n}$ are given by equations (5) and (3) respectively. The explicit expressions for $\{f^{(0)}_\alpha\}$ and $\{g^{(0)}_\alpha\}$ are given in reference [17].

We can derive the differential equations generated by this discrete scheme by scaling the variables and Taylor expanding equations (8) and (9). To second order in Δx this gives [7,18]

$$\partial_t n + \partial_i(nu_i) = 0, \tag{15}$$

$$\partial_t(nu_i) + \partial_j(nu_j u_i) = -\partial_i p_0 + \nu\nabla^2(nu_i) + \xi\partial_i\partial_j(nu_j), \tag{16}$$

$$\partial_t \Delta n + \partial_i(\Delta n u_i) = \Gamma\theta\nabla^2\mu^0_{\Delta n} - \theta\partial_i(\frac{\Delta n}{n}\partial_i p_0). \tag{17}$$

Equation (15) is the continuity equation. Equation (16) is close to the compressible Navier-Stokes equation with viscosities

$$\nu = \frac{(2\tau_f - \Delta t)}{6}v^2 \tag{18}$$

and

$$\xi = \left(2 - \frac{3kT}{v^2}\right)\nu. \tag{19}$$

In the incompressible limit ($n \approx$ const.), equation (16) reduces to the incompressible Navier-Stokes equation.

Equation (17) is the convection-diffusion equation with

$$\theta = \tau_g - \Delta t/2. \tag{20}$$

This form of the convection-diffusion equation, except for the final term, is standard for isothermal systems, where the driving force for diffusion is a gradient in the chemical potential [19] (secs. 58). The final term is believed to be negligible [20]. For example, looking ahead to Section 3.3 we observed no effect on the capillary wave damping when reducing θ (keeping $\Gamma\theta$ constant).

2.3 Two viscosities

To allow the different phases to have different viscosities we choose the relaxation time τ_f to be a function of $\Delta n/n$. For binary mixtures composed of two chemical components several empirical laws have been proposed to relate the viscosity of the solution ν to the viscosity of the components ν_A and ν_B [21]. We choose one of the simplest of these, the so-called "ideal" viscosity of a binary mixture first proposed by Arrhenius [21,22], which in our variables reads

$$\nu = \nu_A^{\frac{n+\Delta n}{2n}}\nu_B^{\frac{n-\Delta n}{2n}}. \tag{21}$$

The exponents correspond to the fraction of components A and B respectively. The relaxation parameter τ_f used in the simulations then follows from equation (18).

The viscosity of the binary mixture varies smoothly with $\Delta n/n$ across the interface, whose thickness is itself determined by the choice of κ. No artificial cut-off values are necessary [10]. We shall use ν_1 and ν_2 to denote the viscosity in bulk phases 1 and 2, respectively.

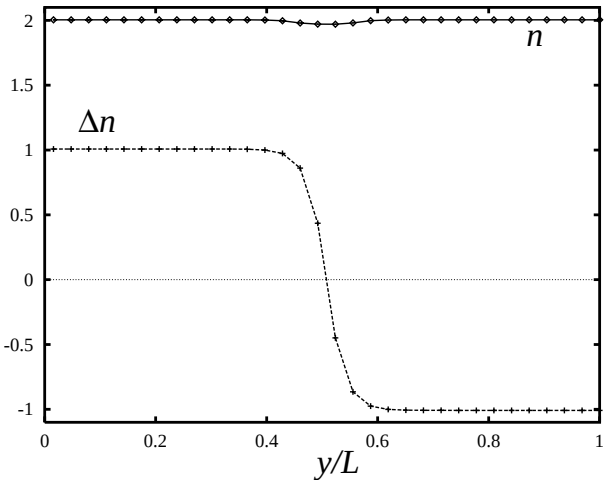

Fig. 1. Profiles for the total density n (full line) and the density difference Δn (broken line) across an interface. Parameters $kT = 0.5$, $\varpi = 1.1$, and $\kappa = 0.04$ are used.

3 Results and discussion

The chemical potential (3) is zero across an equilibrated interface. This determines the solution for Δn across the interface, and the surface tension (7) can be calculated. Wagner [17] obtained a good match when comparing the theoretical surface tension with that calculated from Laplace's law for the pressure difference between the inside and the outside of a drop, simulated by this method. However, for small κ values (thin interfaces), the surface tension found using simulations is somewhat less than that calculated from the theory because of discreteness errors.

In the following we assume $\Delta t = \Delta x = 1$. For $kT = 0.5$, $n = 2$ and $\varpi = 1.1$ we find a theoretical surface tension $\sigma = 0.2217\sqrt{\kappa}$ [17]. Increasing κ increases the surface tension, and also the thickness of the equilibrium interface. Figure 1 shows the variation of n and Δn over an equilibrated interface. Let Δn_0 denote the absolute value of the density difference in the bulk phases. Using $\kappa = 0.04$, the interface thickness is 4-5 lattice spacings. Thus the method is ideal for simulating two-phase problems on a *mesoscopic* scale, where a finite interface-thickness is relevant. For $\kappa = 0$ a sharp interface of one lattice spacing is obtained, but this corresponds to zero surface tension and the equilibrated surface will not be stable to small perturbations.

We now test the model by considering simple flows for which exact results are available. Note however that the analytic results are for two-phase flow with a sharp, not an extended interface. Therefore we do not expect exact agreement in the interface region. All simulations were run with $kT = 0.5$, $n = 2$, $\varpi = 1.1$, $\Gamma = 0.80$, $\tau_g = 1$ and $\kappa = 0.04$ unless other parameter values are specified.

3.1 Shear flow

Consider a two-dimensional fluid flowing in the x-direction with shear imposed in the y-direction. Initially, bulk

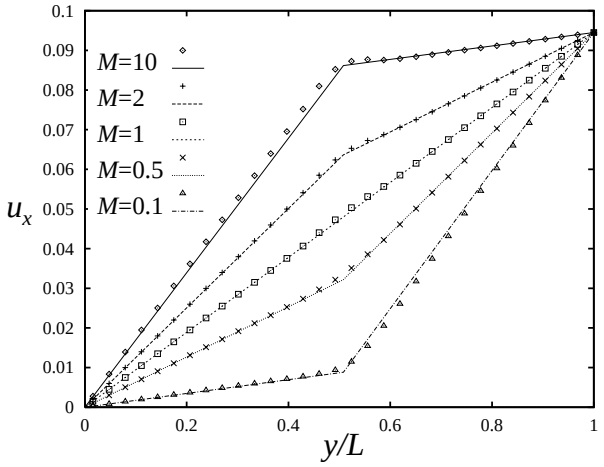

Fig. 2. Velocity in the x-direction u_x as a function of y/L for shear flow. For $0 \leq y/L \leq 0.5$ the density difference is $+\Delta n_0$, for $0.5 \leq y/L \leq 1.0$ it is $-\Delta n_0$. Simulation results (points) and analytical prediction for a sharp interface (lines) are compared for different viscosity ratios M.

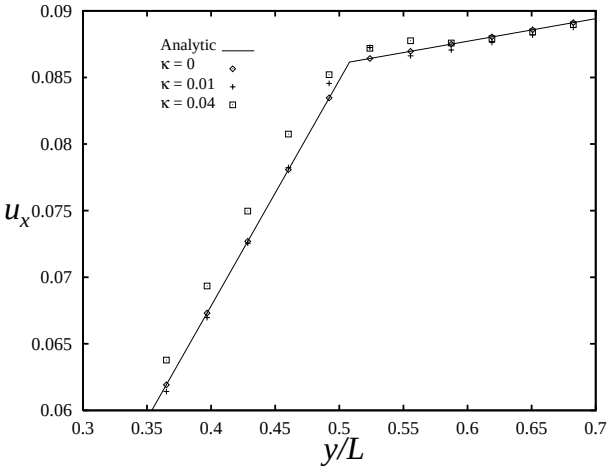

Fig. 3. Velocity in the x-direction u_x as a function of y/L for shear flow. The viscosity ratio (M) equals 10. Simulated results (points) at different κ-values are compared to the analytical prediction for a sharp interface (line).

phase 1, with density difference $+\Delta n_0$, is placed in the space between $y = -L/2$ and $y = L/2$ and bulk phase 2, with density difference $-\Delta n_0$ between $y = -L$ and $y = -L/2$ and between $y = L/2$ and $y = L$. At each time step we impose a constant velocity at $y = \pm L$.

$$\mathbf{u}(y) = \begin{cases} (u_0, 0) & y = L, \\ (-u_0, 0) & y = -L. \end{cases} \tag{22}$$

To simulate this problem we use a system periodic in both directions. The boundary condition equation (22) is imposed by an instantaneous relaxation ($\tau_f = 1$) to the proper equilibrium distribution functions at $y = \pm L$. We take $u_0 = 0.0945v$. To avoid spurious boundary effects, we also use $\tau_f = 1$ in bulk phase 2. The required viscosity ratio is obtained by adjusting the relaxation parameter in phase 1.

Figure 2 shows the variation of the x-component of the velocity u_x for $0 \leq y \leq L$ and different values of the viscosity ratio $M = \nu_2/\nu_1$. The results are compared to the analytic solution for Newtonian fluids

$$u_x(y) = \begin{cases} 2u_0 y[L(1 + \frac{1}{M})]^{-1}, & 0 \leq y \leq L/2, \\ u_0[(2y - L) + ML][L(M + 1)]^{-1}, & L/2 \leq y \leq L. \end{cases} \tag{23}$$

Agreement is excellent. The increasing deviations as M increases/decreases are a consequence of the finite interface width and the choice (21) which allows the viscosity to vary smoothly through the extended interface. Runs with smaller κ, which correspond to a narrower interface, do indeed give results that approach the analytic solution, see Figure 3. The interface is also stable for $\kappa = 0$ because the lattice Boltzmann algorithm contains no intrinsic noise. For longer runs the noise due to round-off errors may destabilise the $\kappa = 0$ interface.

Figure 2 does, however, reveal a small unphysical effect in the model. For $M = 1$ the velocity profile varies slightly from linear in the region of the interface ($\sim 1\%$). This is due to the small change in the total density n across the interface ($\sim 1.7\%$ for the parameters used here). The 9-velocity lattice Boltzmann model becomes non-Galilean-invariant for compressible flow: more velocities would be needed to correct for this.

3.2 Poiseuille flow

We next consider Poiseuille flow in the x-direction. We used the same starting configuration for the fluid as for shear flow. Non-slip walls at $y = \pm L$ are imposed by using "bounce back" boundary conditions with the walls placed half way between the nodes. This scheme is of second-order accuracy in the lattice spacing for simple flows [23]. Periodic boundary conditions are imposed in the x-direction and a body force drives the flow.

The analytical solution for a sharp interface is

$$u_x(y) = \begin{cases} \frac{1}{2}G[(L^2/4 - y^2)/\nu_1 + \frac{3}{4}L^2/\nu_2], & 0 \leq y \leq L/2, \\ \frac{1}{2}G(L^2 - y^2)/\nu_2, & L/2 \leq y \leq L, \end{cases} \tag{24}$$

where G is the imposed force [24].

This solution is compared to our numerical results in Figure 4. Again there is close agreement for most cases. However there is a pronounced discrepancy in the high viscosity phase for $M = 10$, the largest value considered. This is a physical result arising from the finite interface width: the numerical results approach the analytic ones as expected as the width of the interface decreases [25].

3.3 Capillary waves

As a dynamic test of the model capillary waves were investigated. The system consisted of walls at $y = 0$ and $y = H$

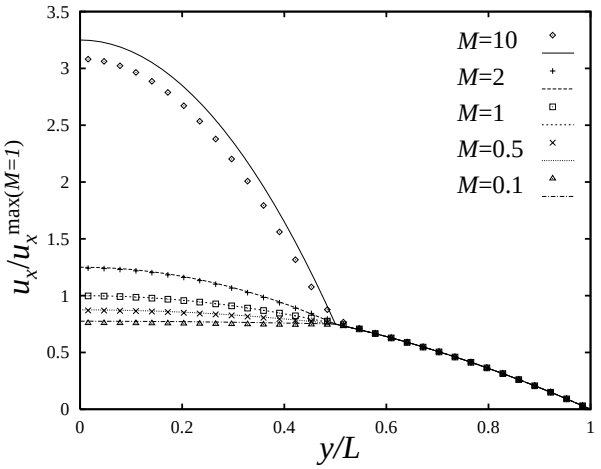

Fig. 4. Velocity in the x-direction u_x (relative to the theoretical maximum velocity for $M = 1$) as a function of y/L for Poiseuille flow. For $0 \leq y/L \leq 0.5$ the density difference is $+\Delta n_0$, for $0.5 \leq y/L \leq 1.0$ it is $-\Delta n_0$. Simulation results (points) and analytical prediction for a sharp interface (lines) are compared for different viscosity ratios M.

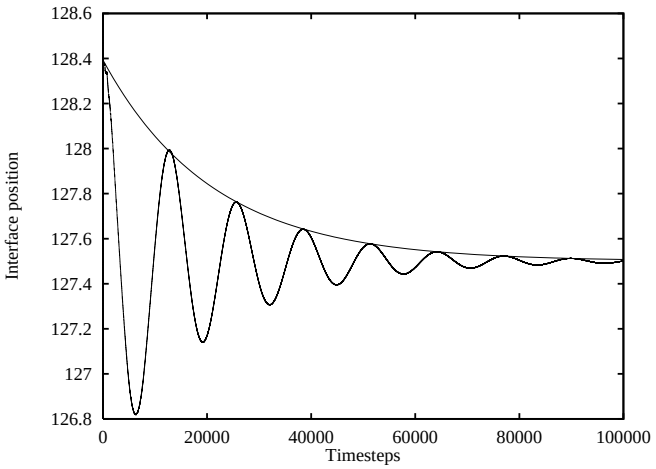

Fig. 5. The y-position of the capillary wave interface as a function of time (dots). An exponential curve is fitted to the peak points (line).

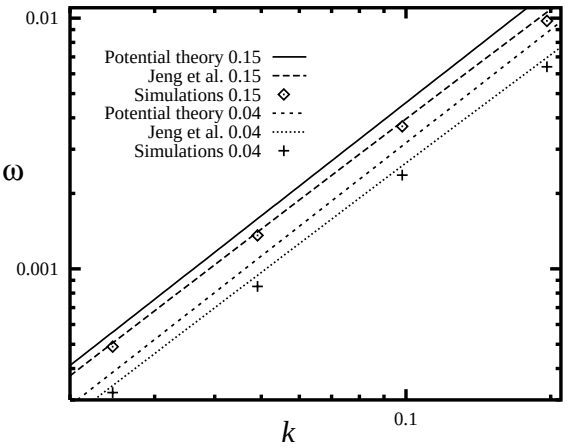

Fig. 6. The dispersion relation (angular frequency ω *vs.* wave number k). Simulations using $\kappa = 0.15$ and $\kappa = 0.04$ are compared with the corresponding analytical solutions from potential theory and from Jeng *et al.* [26].

while it was periodic in the x-direction. The wave was initialized as a sinusoidal curve around $y = H/2$ of one wavelength L and amplitude a separating the two bulk phases. The system was then allowed to relax to equilibrium under the influence of capillary and viscous forces only (no gravity). The result was a damped standing wave. At each timestep, at a certain x-value, the height of the interface was measured. This curve was used to find the oscillation frequency as well as the damping of the wave. To not complicate the problem further, the same viscosity was used in the two phases ($M = 1$).

The classical analytical treatment of such a wave is based on potential flow theory and ideal fluids, see *e.g.* reference [19]. Jeng *et al.* [26] recently extended the analysis to a wave between two viscous fluids. Both derivations assume a small amplitude a, $a/L \ll 1$ such that the non-linear term in the Navier-Stokes equation can be neglected. Also, Jeng *et al.*'s results hold only for large liquid depths.

Jeng *et al.*'s solution is complicated but converges to that of potential flow theory,

$$\omega = \sqrt{\frac{\sigma k^3}{2n}}, \qquad \gamma = 2\nu k^2 \tag{25}$$

when the viscosities go to zero. Here, ω is the angular frequency, k the wavenumber and γ the damping coefficient of the capillary waves. Both the Jeng *et al.* result and the potential flow result are compared to the lattice Boltzmann results below.

Parameters $a/H = 0.02$ and $H = 256$ were found to be appropriate for this study. A viscosity parameter $\tau_f = 0.7$ was used in the simulations. Both a high ($\kappa = 0.15$, interface width ~ 10) and a low ($\kappa = 0.04$, interface width ~ 4–5) surface tension were used. Wavelengths $L = 256$, 128, 64 and 32 all gave a damped wave motion with uniform periods and peaks which fit perfectly to an exponential curve determining the damping coefficient. Figure 5 shows the damped wave motion and the fit to an exponential curve $e^{C-\gamma t}$ for $\kappa = 0.15$ and $L = 256$.

The mean of typically the 8 first periods was used to calculate the angular frequency. In Figure 6 the frequencies obtained are plotted against $k = 2\pi/L$. For comparison the analytical dispersion relations are also given. The surface tension used in the analytical formulae, is the one found from Laplace law corresponding to the κ value. For $\kappa = 0.15$ a good quantitative match to the solution of Jeng *et al.* is obtained at low wave numbers. At high values of k (short wavelength L) the assumption $a/L \ll 1$ holds less well and non-linear effects becomes more important. Therefore it is reasonable to expect discrepancies

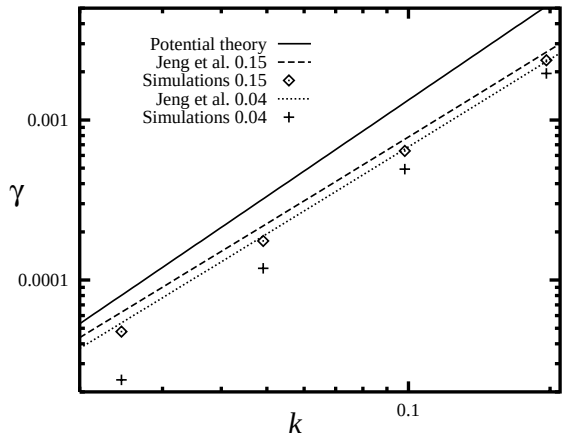

Fig. 7. The damping coefficient γ as a function of the wave number k. Simulations using $\kappa = 0.15$ and $\kappa = 0.04$ are compared with the corresponding analytical solutions from potential theory and from Jeng *et al.* [26].

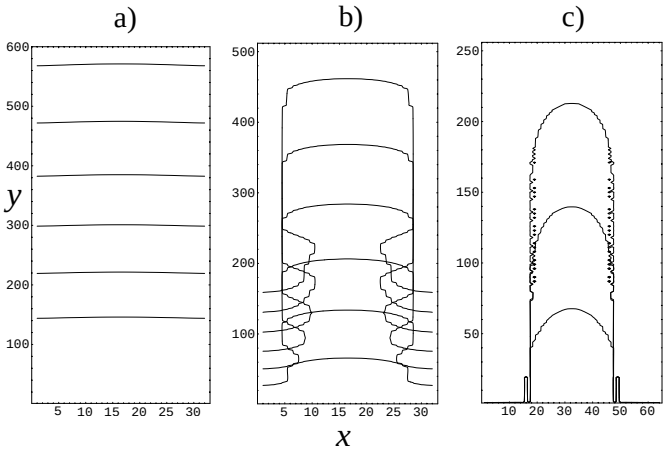

Fig. 8. Finger evolution for $M = 10$ and $\bar{u} = 0.01$. a) $\kappa = 0.04$, t (from bottom) $= 2n \times 10^4 \Delta t$, $n = 2, 3 \ldots 7$. b) $\kappa = 0.01$, $t = n \times 10^4 \Delta t$, $n = 1, 2 \ldots 6$. c) $\kappa = 0$, $t = 5n \times 10^3 \Delta t$, $n = 1, 2, 3$.

with the numerical results which do take account of the non-linearities in the Navier-Stokes equations. This is the same effect as detected by others [4]. For our choice of H we find a better match to Jeng *et al.*'s solution at $L = 128$ (3.0%) as compared to $L = 256$ (3.3%). This is likely to be because the theory also assumes $H/L \gg 1$. Doubling H to 512 at $L = 128$ (keeping the same absolute size of the amplitude) reduced the discrepancy to 2.9%.

Using $\kappa = 0.04$, the fit to Jeng *et al.*'s result is again best at low wave numbers, but the discrepancy is somewhat larger as compared to the $\kappa = 0.15$ simulations. *E.g.*, the relative discrepancy to Jeng *et al.*'s result is now 6.2% and 9.8% at $L = 256$ and $L = 128$, respectively. It is reasonable that a larger discrepancy is obtained with the thinner interface because the basic assumption of smooth gradients [13] underlying equation 2 itself becomes less correct.

For each wave an excellent match was obtained when fitting the peak data-points to an exponential curve $\mathrm{e}^{C-\gamma t}$. (The initial peak point was not used in the fitting procedure.) Figure 7 shows the damping coefficient γ obtained for various k. Again our results compare much better to the solution of Jeng *et al.* than to that predicted by pure potential flow theory. The damping found using simulations is however less than both the theoretical ones. The damping shows a larger difference to Jeng *et al.*'s result as compared to the dispersion relation. The relative discrepancy to Jeng *et al.*'s result increase with decreasing k. This trend was found not to be sensitive to the size of H/L nor the Γ parameter (which was used to minimize the effect of the second term in Eq. (17)). We believe this behaviour is caused by the lack of Galilean invariance in the interface region, as discussed in Section 3.1.

3.4 Fingering in two dimensions

We now use the two-viscosity lattice Boltzmann method to investigate fingering. One phase pushes the second, M times more viscous, along a two-dimensional channel with non-slip walls at $y = 0$ and $y = W$. The driving fluid forms a growing finger if M and the capillary number Ca defined by

$$Ca \equiv \frac{u_t n \nu_2}{\sigma} \tag{26}$$

are large enough. In this definition u_t is the velocity at the tip of the finger and ν_2 is the kinematic viscosity of the displaced fluid.

The non-slip condition is imposed as in Section 3.2. Initially, only bulk phase 2 is present in the channel. The injection of phase 1 is implemented as simply as possible. At each time step, following the streaming and collision operations, the first x-column is set to contain bulk phase 1 and the last x-column to contain bulk phase 2, both with a wanted mean velocity $\bar{u}$. To avoid unnecessary boundary effects, a Poiseuille profile (along y) for the in/out velocities is used. The scheme produces a build-up of the pressure close to inlet and a build-down of the pressure close to outlet. This pressure gradient drives the flow. (Using this method, the actual mean velocity in the channel is somewhat lower than $\bar{u}$.) The time needed to establish a stable finger varied for the different capillary numbers used. Grid-sizes of (512×32), (1026×32), and (512×64) were appropriate.

Figure 8 shows the evolution of fingers having $M = 10$ and $\bar{u} = 0.01v$. The fingers are represented by the contour line $\Delta n = 0$ and are plotted at equal time intervals. As time evolves the fingers move upwards in the figure. The viscosity ratio $M = 10$ is obtained by choosing $\tau_f = 0.6$ and 1.5 in bulk phases 1 and 2 respectively. With such values of τ_f and $W = 32\Delta x$ one-phase Poiseuille flow is reproduced to 0.3% [23]. Hence we expect no error associated with the non-slip boundaries. In Figure 8a $\kappa = 0.04$.

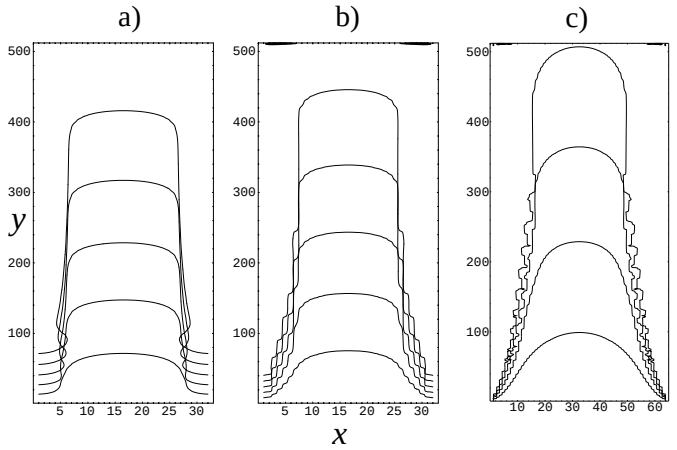

Fig. 9. Finger evolution for $M = 10$ and $\bar{u} = 0.1$. a) $\kappa = 0.04$, $t = n \times 10^3 \Delta t$, $n = 1, 2 \ldots 5$. b) $\kappa = 0.01$, $t = n \times 10^3 \Delta t$, $n = 1, 2 \ldots 5$. c) $\kappa = 0$, $t = n \times 10^3 \Delta t$, $n = 1, 2, 3, 4$.

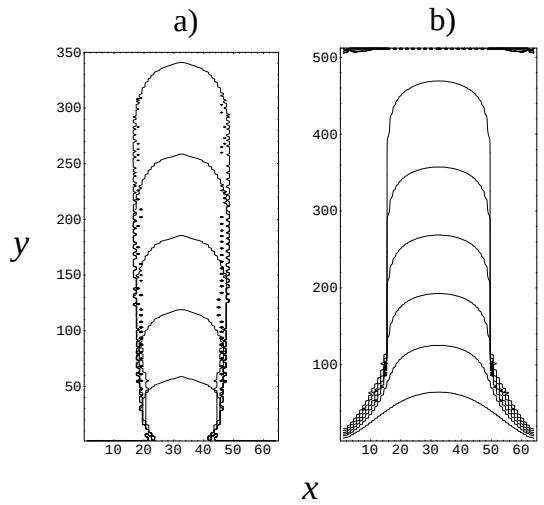

Fig. 10. Finger evolution for $\kappa = 0$ and $M = 100$. a) $u = 0.01$, $t = n \times 10^4 \Delta t$, $n = 1, 2 \ldots 5$. b) $u = 0.1$, $t = n \times 10^3 \Delta t$, $n = 1, 2 \ldots 6$.

For this high value of the surface tension no finger is observed in a (512×32) or a (1024×32) system. In Figure 8b $\kappa = 0.01$, which produces a stable finger. The interface is quite sharp and the step-like behaviour of the finger profiles is a consequence of the finite lattice resolution and will smooth out with an increased lattice size. Figure 8c has $\kappa = 0$ and there is no longer any energy associated with the interface. One might expect the interface to be unstable and there are some signs that smaller side-fingers are being formed by the end of the simulation. Lattice Boltzmann simulations include no intrinsic noise and the small perturbations caused by the round off errors (of order 10^{-16}) do not have enough time to grow.

Figures 9a, b, and c show results for the same three values of κ but for a larger driving velocity $\bar{u} = 0.1v$. For $\kappa = 0.04$ (a) a smooth stable finger is formed. For lower κ (b,c) instabilities again occur but now only at the back of the finger. Figures 8b and 9a have an indented part near the beginning of the fingers.

Table 1. Summary of the data obtained from the finger simulations.

M	$\bar{u}(v)$	κ	$u_t(v)$	Ca	$u_t^{\mathrm{err}}(\%)$	λ
10	0.01	0.04	0.0048	0.079	6.9	1.00 ± 0.03
10	0.01	0.01	0.0094	0.39	10	0.75 ± 0.03
10	0.01	0	0.015	∞	0.9	0.466 ± 0.016
10	0.1	0.04	0.098	1.6	9.9	0.64 ± 0.03
10	0.1	0.01	0.11	4.6	11	0.56 ± 0.03
10	0.1	0	0.14	∞	5.1	0.529 ± 0.016
100	0.01	0	0.0082	∞	11	0.501 ± 0.016
100	0.1	0	0.11	∞	21	0.531 ± 0.016

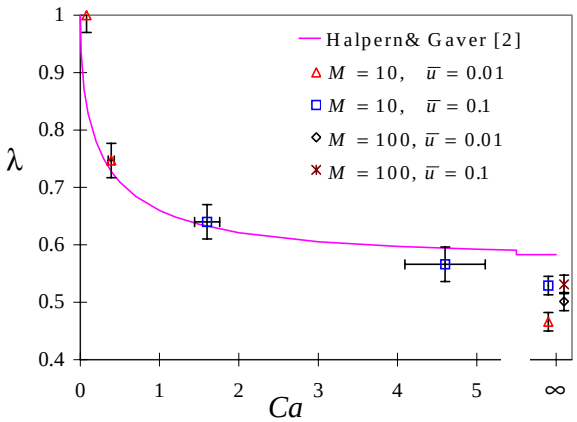

Fig. 11. Finger-width as a function of capillary number Ca. The results of Halpern and Gaver [2] are shown for comparison.

Figure 10 shows results for a larger viscosity difference $M = 100$ and $\kappa = 0$ for two different values of $\bar{u}$. $M = 100$ is achieved by increasing τ_f to 10.5 in bulk phase 2. The bounce-back conditions at the wall are not ideal for such high relaxation times in general, giving a slip-condition [27]. For these two cases however, bulk phase 2 behind the tip of the finger does not flow at all and thus the boundary conditions should not introduce any significant errors. The finger shape is virtually unaffected by the higher viscosity ratio (compare Fig. 10a with 8c and 10b with 9c).

The results of the simulations for different values of the viscosity ratio M, the tip velocity u_t, and the surface tension κ are summarised in Table 1. Here, λ is the width of the finger relative to W, the width of the cell. Capillary numbers are based on the measured tip-velocities (u_t) of the fingers, read directly from the figures, and the surface tension found from Laplace law. Table 1 gives the measured data with uncertainty-estimates. The uncertainty in u_t, and thereby Ca, is based on the relative change between the two last measurements of u_t. The uncertainty in λ is given as one lattice spacing. The results in the table are presented graphically in Figure 11 where they are compared to those obtained by other authors.

We now summarise previous work on two-dimensional fingering and list possible reasons for the discrepancies found. Reinelt and Saffman [1] presented a finite difference solution of the Stokes problem in two dimensions. The highest capillary number they consider was 2, with a corresponding $\lambda \approx 0.62$. Halpern and Gaver [2] extended the study looking at the translation of a two-dimensional bubble in a channel. Their boundary element solution matched the result of Reinelt and Saffman but extended the solution to higher Ca. Their result are shown as the line in Figure 11. In particular λ_∞ was predicted to 0.583. Here the ∞ subscript means at the limit of high Ca.

Except for a small discrepancy for the smallest Ca reported, Figure 11 shows that we reproduce the results of Reinelt and Saffman ($Ca < 2$). For $Ca > 2$ we find a smaller λ than Halpern and Gaver. In particular we find a lower value for λ_∞.

There are several possible reasons for the discrepancies. It may be that the fingers in our simulations have not attained their steady state although all the checks we performed suggested that this was not the case. Discrepancies with Halpern and Gaver's result may also occur because they use an idealized fluid description which neglects among other things the non-linear term in the Navier-Stokes equation. On the other hand, correction terms in the lattice Boltzmann approximation to the Navier-Stokes equations may affect our numerical results. Such corrections terms are probably the reason for the small dependence of λ_∞ on $\bar{u}$ that we observe (see Fig. 11). Another explanation, discussed in Section 3.3, is that the basic assumption of smooth gradients [13] underlying equation (2) itself becomes less correct as we decrease the interface thickness.

Moreover the previous results are for $M = \infty$ whereas our simulations are for finite M. As we increase M from 10 to 100 only the low-velocity finger is affected (λ_∞ is changed from 0.47 to 0.50). Rakotomalala *et al.* [11,12] studied fingering of miscible fluids in a 2D channel. At high Péclet numbers (ratio of viscous to diffusive forces) their result should be similar to our immiscible problem. In this limit and large M they found $\lambda \approx 0.56$. Their simulated fingers were almost identical for $M = 100$ and $M = 1000$.

4 Summary

A thermodynamically consistent model for the simulation of a binary fluid has been extended to handle different viscosities. The model is ideal for simulating two-phase flow on a *mesoscopic* scale, where the interface between the phases has a finite thickness. It is also possible to obtain results in the limit of zero interface thickness. Hence we expect the approach to be useful in problems such as the simulation of multiphase flow in the pore-space of a porous medium, spinodal decomposition in fluids with a dynamic asymmetry, or simulation of more complex fluids such as microemulsions where the differing viscosity of the phases may have a significant effect on the rheology.

The method was used to study shear and Poiseuille flow in layered fluids. We obtained good agreement with the analytic solutions given that the latter are for interfaces of zero width.

As a further check of the model the evolution of a capillary wave were investigated. The dispersion relation compared very well to analytical predictions in reference [26]. Agreement becomes less good for large k where the simulations are able to account for non-linear effects. Good agreement persisted even for interfaces as narrow as $\sim 4-5$ lattice spacings. The amplitude of the simulated wave relaxed as a perfect exponential and the damping coefficient found compared qualitatively well to the analytical predictions in reference [26] but was somewhat smaller.

Finally, the model was applied to simulate the displacement of a fluid by a less viscous fluid in a two-dimensional channel. The simulated finger width agreed quantitatively with previous numerical work at capillary numbers below 2. For $Ca > 2$ however, our method predicts a smaller finger width than found in the one previous study. A limiting finger width close to $1/2$ is obtained for high capillary numbers and high viscosity ratios.

We would like to thank P. Papatzacos, A. Wagner and S. Ekrann for helpful discussions. This work has received support from the Research Council of Norway (PROPETRO and the Programme for Supercomputing) through a Ph.D.-grant and computing time on the Origin 2000 at Parallab, Bergen.

References

1. D.A. Reinelt, P.G. Saffman, SIAM J. Sci. Stat. Comput. **6**, 542–561 (1985).
2. D. Halpern, D. P. Gaver, J. Comp. Phys. **115**, 366–375 (1994).
3. R. Benzi, S. Succi, M. Vergassola, Phys. Rep. **222**, 145–197 (1992).
4. A.K. Gunstensen, D. Rothman, S. Zaleski, G. Zanetti, Phys. Rev. A **43**, 4320–4327 (1991).
5. E.G. Flekkøy, Phys. Rev. E **47**, 4247–4257 (1993).
6. E. Orlandini, M.R. Swift, J.M. Yeomans, Europhys. Lett. **32**, 463–468 (1995).
7. M.R. Swift, E. Orlandini, W.R. Osborn, J.M. Yeomans, Phys. Rev. E **54**, 5041–5052 (1996).
8. A.J. Wagner, J.M. Yeomans, Phys. Rev. Lett. **64**, 3732–3747 (1998).
9. K. Langaas, D. Grubert, in *Proceedings from the 5'th International Symposium on Evaluation of Reservoir Wettability and its Effect on Oil Recovery, 22-24 June 1998*, (Extended version to be published in J. Petr. Sci. Engng.).
10. D. Grunau, S. Chen, K. Eggert, Phys. Fluids A **5**, 2557–2562 (1993).

11. N. Rakotomalala, D. Salin, P. Watsky, J. Fluid Mech. **338**, 277–297 (1997).
12. N. Rakotomalala, D. Salin, P. Watsky, J. Phys. II France **7**, 967–972 (1997).
13. J.S. Rowlinson, B. Widom, *Molecular Theory of Capillarity* (Clarendon Press, Oxford, 1984).
14. A.J.M. Yang, P.D. Fleming, J.H. Gibbs, J. Chem. Phys. **64**, 3732–3747 (1976).
15. H. Chen, S. Chen, W.H. Matthaeus, Phys. Rev. A **45**, 5339–5342 (1992).
16. Y.H. Qian, D. d'Humières, P. Lallemand, Europhys. Lett. **17**, 479–484 (1992).
17. A. Wagner, *Theory and Applications of the Lattice Boltzmann Method*, Ph.D. thesis, University of Oxford, 1997.
18. K. Langaas, *Modelling of Immiscible Two-Phase Flow in Porous Media with the Binary Fluid Lattice Boltzmann Method*, Ph.D. thesis, University of Bergen, Norway, 1999.
19. L.D. Landau, E.M. Lifshitz, *Fluid Mechanics*, 2nd ed. (Pergamon press, Oxford, 1987).
20. E. Orlandini, private communication.
21. J. Barthel, M. Utz, K. Groß, H.-J. Gores, J. Sol. Chem. **24**, 1109–1123 (1995).
22. L. Grunberg, A.H. Nissan, Nature **164**, 799–800 (1949).
23. X. He, Q. Zou, L.S. Luo, M. Dembo, J. Stat. Phys. **87**, 115–136 (1997).
24. R.B. Bird, W.E. Stewart, E.N. Lighfoot, *Transport Phenomena*, (Wiley, New York, 1960).
25. K. Langaas, in *Proceedings from the 6'th European Conference on the Mathematics of Oil Recovery, 8-11 Sept. 1998* (The Hague, 1998), EAGE, pp. 1–10.
26. U.S. Jeng, L. Esibov, L. Crow, A. Steyerl, J. Phys. Cond. Matter **10**, 4955–4962 (1998).
27. T. Inamuro, M. Yoshino, F. Ogino, Phys. Fluids **7**, 2928–293 (1995).